



Synthesis of CuO hollow nanoparticles using laser ablation: effect of fluence and solvents

Rajesh Rawat¹ · Archana Tiwari¹ · Nimmala Arun^{2,3} · S. V. S. Nageswara Rao^{2,3} · A. P. Pathak^{1,2} · S. Venugopal Rao⁴ · Ajay Tripathi¹

Received: 2 January 2020 / Accepted: 11 February 2020
© Springer-Verlag GmbH Germany, part of Springer Nature 2020

Abstract

Nanosecond laser pulses (1064 nm, 8 ns and 10 Hz) were employed to ablate a Cu target immersed in deionized water (DI) and ethylene glycol (EG). The ablation process was carried out for 60 min for two different laser fluences, i.e., 27 J/cm² and 80 J/cm², which resulted in the formation of Cu/CuO nanoparticles (NPs) in both the media. The effects of laser fluence and solvents on the morphology of NPs were investigated using structural and optical characterization techniques (such as TEM, HRTEM, XRD, UV–visible and PL spectroscopy). The colloidal solution synthesized at the low fluence of 27 J/cm² in DI illustrated the presence of hollow structured CuO NPs and has been attributed to the Kirkendall effect. At the high fluence of 80 J/cm², porous NPs were seen which has been attributed to the dissolution of H₂ molecules. In EG, no signature of hollow or porous NPs was seen and this has been accredited to its oxygen deficiency and viscous nature. Additionally, the growth kinematics involved in the transformation of morphology are elaborately discussed.

Keywords Laser ablation · Fluence · Cu/CuO NPs · Hollow NPs · Kirkendall effect · Hydrogen dissolution

1 Introduction

Hollow nanoparticles (HNPs) have gained tremendous interest among the researchers because of their unique properties such as high-surface-to-volume ratio, low density and extensive use in the application area of batteries, drug delivery, thermal insulation, photo-catalytic activity and so on [1–3]. There are various synthesis techniques (e.g., chemical and

physical methods) for HNPs' generation, reported in the recent literature [4–7]. Among these, hollow/porous NPs synthesized using pulsed laser ablation (PLA) technique have attracted appreciable attraction in recent years, in the field of nanomaterials. The reason behind the attention toward PLA technique is due to its feasibility and environmental-friendly process as compared to chemical synthesis which requires harmful chemical reagents. In addition, the advantages of using PLA technique are that the size, shape and morphology of the as-synthesized NPs are found to be dependent on laser parameters (laser pulse energy, pulse duration, repetition rate, laser wavelength, laser ablation time, focusing distance, target-to-liquid-surface distance), on target material and on the physical properties of liquid environment (such as polarity, thermal conductivity, density and viscosity) [1, 8–17], which makes it a reliable candidate over chemical techniques. Recently, Zhang et al. [2] reported the formation of hollow cobalt (Co) NPs using single-shot nanosecond laser ablation of Co target in water and ethanol with varying laser beam spots and laser pulse energies. They proposed that a possible mechanism for the formation of hollow NPs (HNPs) was via diffusive thermochemical reactions or bubble-assisted mechanism. Nakamura et al. [18], Wang et al. [19] and Yin et al. [20] reported the formation of HNPs

Electronic supplementary material The online version of this article (<https://doi.org/10.1007/s00339-020-3403-1>) contains supplementary material, which is available to authorized users.

✉ Ajay Tripathi
ajay_t_2000@yahoo.com

¹ Department of Physics, School of Physical Sciences, Sikkim University, Tadong, Sikkim 737102, India

² School of Physics, University of Hyderabad, Hyderabad 500046, India

³ Center for Advanced Studies in Electronic Sciences and Technology (CASEST), School of Physics, University of Hyderabad, Hyderabad 500046, India

⁴ Advanced Center of Research in High Energy Materials (ACRHEM), University of Hyderabad, Hyderabad 500046, India

in Al and Cu, Fe and Co via the Kirkendall voiding effect. They reported that this effect is applicable only with the metals having high diffusion coefficient as compared to their oxides shell. The Kirkendall effect is initiated during the oxidation of a metallic particle where the outward diffusion of metal core is rapid as compared to inward diffusion of its oxides shell. Fan et al.[4] also reviewed the formation of HNPs via the Kirkendall effect in various metal systems such as Zn, Al, Fe and Co. Niu et al.[21] discussed the formation of HNPs in Zn, Mg, Fe, Co, Ni, Cu, Pb and Ti systems via the Kirkendall effect and selective heating of the core with an infrared laser. Kuzmin et al.[22] discussed the generation of Al and Ti HNPs via bubble-assisted mechanism in hydrogen-saturated solvents (i.e., ethanol, n-propanol and water). They reported that during the PLA process the surrounding liquid undergoes optical breakdown (formation of vaporized bubble) together with the ejection of particles from the surface. In the process of bubble expansion, an appreciable number of NPs get trapped at the vaporized bubble interface, resulting in the formation of HNPs. Similarly, Yan et al.[23–25] also observed the bubble-assisted generation of HNPs in Al, Mg and Zn systems.

Out of all the metals investigated, there are very few reports on the synthesis of hollow Cu/CuO NPs using PLA [26–28]. This is due to the high reactivity of Cu that reacts with the oxygen molecules present in the solvents and gets oxidized fast, which results in agglomeration of synthesized NPs. Further, the results reported in the literature are either broad or lack in discussing the exact mechanism. Although PLA is a sensitive technique and involves complex phenomena, a small change in the liquid and laser parameters drastically influences the final product of the as-synthesized NPs. In our previous work [28], we have reported the synthesis of Cu/CuO HNPs in ethanol that is a hydrogen-saturated solvent. The suggested mechanism for the formation of HNPs was: (i) dissolution of H_2 and (ii) selected evaporation of Cu core because of multiple interaction of the particles with laser. In this work, we systematically investigated the effects of fluence and solvent on the formation of hollow Cu/CuO NPs. We report the results obtained for two different fluences of 27 J/cm^2 and 80 J/cm^2 with DI and EG as solvents. Based on the results, a detailed mechanism has been proposed.

2 Materials and methods

The copper (Cu) NPs were synthesized by ablating the Cu target (purity 99.99 %), which had a dimension of $13\text{ mm} \times 13\text{ mm}$ and thickness of 0.82 mm in two different solvents. The solvents in which the ablation was carried out in the present study were deionized water (18 M Ω cm at room temperature) and ethylene glycol (henceforth the above solvents are abbreviated as DI and EG), which are purchased

from Merck, India, and were used directly without further purification. Ablation process of Cu target was carried out by placing it at the bottom of the beaker filled with 8 ml of solvent in both cases. The distance from the target to liquid surface was kept at 6 mm throughout the experiment. A Nd:YAG laser (Litron Laser, LPY 707G-10) operating at 1064 nm with 8-ns pulse duration and a repetition rate of 10 Hz was employed for laser ablation of Cu target. A detailed experimental setup is shown in Fig. 1.

Laser pulse energies of 40 mJ and 120 mJ were used for laser ablation, which was focused on the surface of Cu target using quartz lens (150 mm focal length) with a measured spot area of $1.5 \times 10^{-3}\text{ cm}^2$ in both cases. The corresponding ablation fluence measured at the above-mentioned energies is found to be 27 J/cm^2 and 80 J/cm^2 , respectively. The duration of laser ablation was kept fixed at 60 min. During the process of laser ablation, the target immersed in solvent was moved manually in all directions to avoid crater formation. Also, the solvent was continuously stirred with the help of magnetic stirrer at 1020–1030 rpm, so that the synthesized NPs are properly dispersed in the solvent. To maintain the whirling motion without muddling the height of 6 mm between the target and the liquid surface, the magnetic bead was kept at the corner of the beaker as shown in Fig. 1. Before ablating the target, it was cleaned by ultrasonication in acetone for 45 min to remove surface impurities. The target was independently ablated in both the media with 27 J/cm^2 and 80 J/cm^2 . The colloidal solution of the synthesized NPs was then collected for characterization.

The prepared colloidal solution of Cu NPs was examined using spectroscopic and microscopic techniques. The

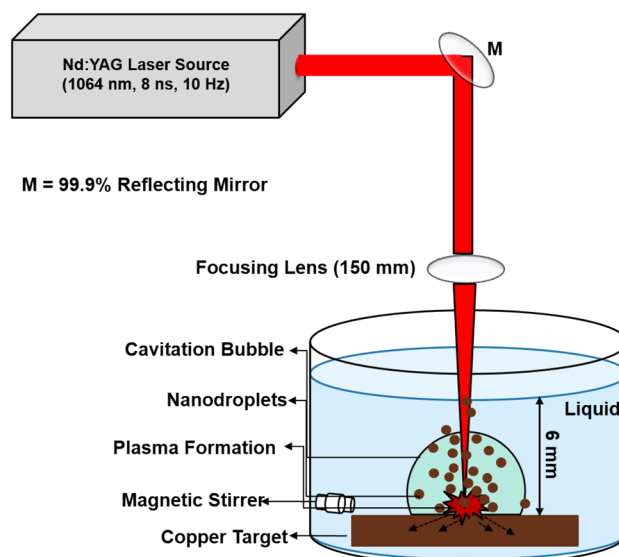


Fig. 1 Experimental setup for the synthesis of Cu NPs by laser ablation

optical response of the synthesized NPs was recorded using UV–Vis (PerkinElmer Lambda 750) spectrometer in the range of 220–900 nm, and photoluminescence (PL) spectra were recorded by PerkinElmer LS55 spectrometer at the excitation wavelength of 275 nm. Structural examination on the prepared samples was done by transmission electron microscopy (TEM). For this, the colloidal solution of NPs was dispersed onto the carbon-coated copper grid and dried. Afterward, high-resolution TEM (HRTEM) and TEM micrographs of the samples were captured using TEM, Tecnai, equipped with thermionic electron gun working at 200 kV. Estimation of average size of NPs obtained from TEM micrographs was measured using GATAN Microscopy Suite software and Digital Micrograph. The X-ray diffraction pattern (XRD) of the samples was recorded using PANalytical XPert Pro XRPD with $\lambda = 1.5406 \text{ \AA}$ of CuK α line.

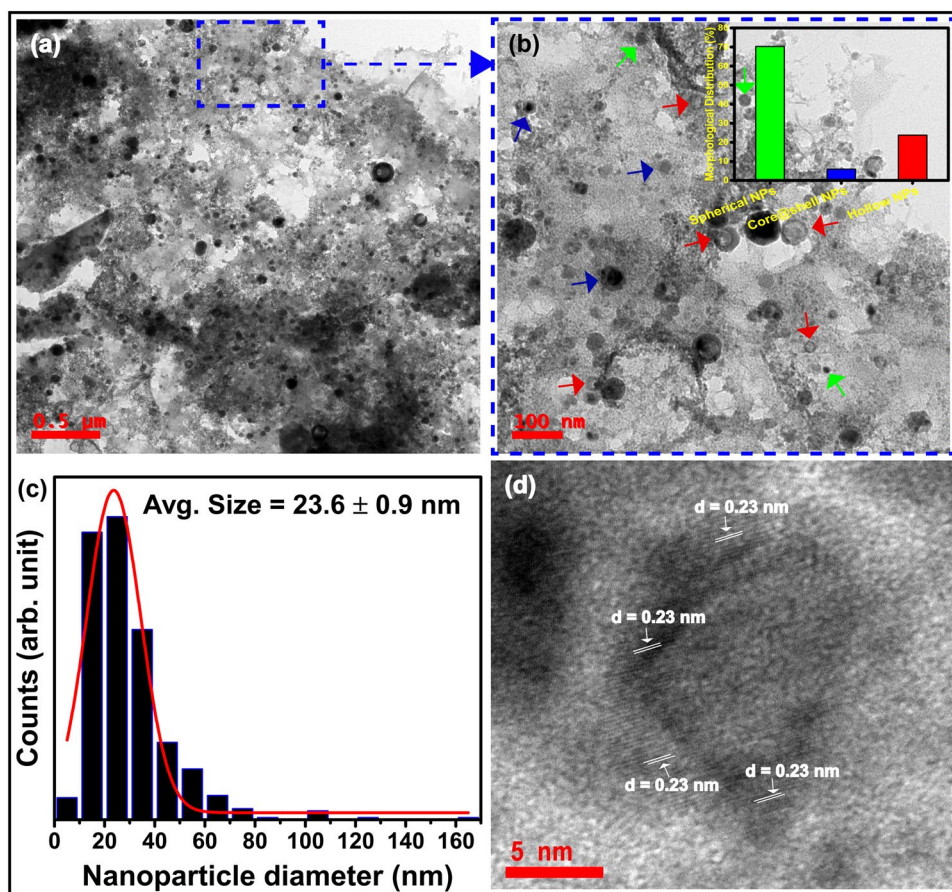
3 Results and discussion

3.1 Structural characterization

3.1.1 TEM analysis

The structural analysis of the samples obtained by ablating Cu target for 60 min in DI and EG with the laser fluence of 27 J/cm^2 and 80 J/cm^2 is shown in Figs. 2, 4 and 5. In Fig. 2a, b, TEM micrographs of samples synthesized at 27 J/cm^2 are shown, which are spherical in nature with an average particle size of $23.6 \pm 0.9 \text{ nm}$. [A corresponding size distribution is shown in Fig. 2c.] On examining the sample, solid spherical NPs together with core–shell and hollow structured NPs (HNPs) have been observed. In Fig. 2b, the presence of core–shell NPs and HNPs is shown, which are indicated with a blue and red solid line arrows, and the morphological distribution is shown in the inset of Fig. 2b. We have analyzed 101 particles out of which 70% of the particles are spherical, 6% are core–shell and 24% possess hollow morphology. The size of HNPs ranged from 6 nm to 60 nm with an average size of $22.8 \pm 3.1 \text{ nm}$. The observed core–shell NPs have the size in the range of 12–32

Fig. 2 (a) and (b), TEM micrographs of Cu particles synthesized at 60-min ablation with laser fluence of 27 J/cm^2 in DI. Insets of figure (b) show the morphological distribution of NPs. (c) The size distribution of the NPs. (d) HRTEM image of single HNPs synthesized in DI at 27 J/cm^2

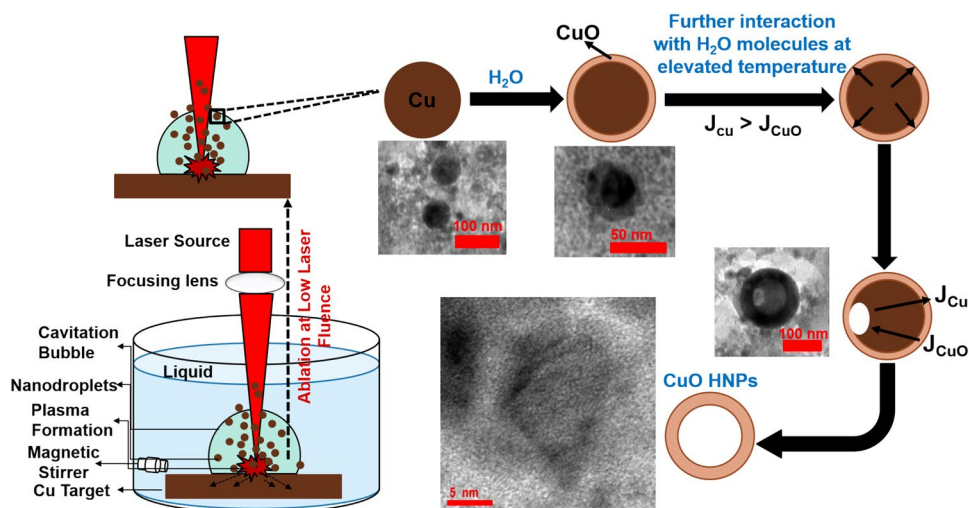


nm with the thickness of shell in the range between 4 and 10 nm. The measured values of the thickness of shell are shown in supplementary figure S1.

In our case, at low fluence, we attribute the formation of HNPs to the Kirkendall effect. Till date, various mechanisms were proposed for the formation of HNPs in laser ablation, viz. bubble-assisted soft templating (BAST) process, selective core evaporation (SCE), dissolution of H_2 molecules and the Kirkendall effect [2, 21, 23]. In BAST process, cavitation bubbles provide the template to form HNPs and has two major requisites: larger life time of bubble and (ii) high concentration of NPs, which are not fulfilled at low fluence [23, 24]. In SCE, the formation of HNPs to take place the two major conditions was laid out: (i) the melting point of the shell should be larger than the boiling point of the core and (ii) the band gap of the shell should be larger than the laser photon energy [21]. Although, in our case, the band gap of shell is more than the photon energy, the melting point of shell is less than the boiling point of core. So, it is expected that we should be seeing features of damaged shell in our case, which were not seen. The third proposed scheme is the formation of void because of the dissolution of H_2 in metal followed by its release in condensation [2, 4, 18, 21]. Although DI is a hydrogen-saturated medium, the low fluence of 27 J/cm^2 which translated into average value of $3.38 \times 10^9 \text{ W/cm}^2$ is not sufficient for breakdown. Considering the ablation time of 60 min, the presence of H_2 cannot be ruled out, but the number will not be sufficient to saturate the NPs. Arguably, the preferential mechanism of the formation of HNPs at low fluence would be the Kirkendall effect, which can be explained as follows: The presence of smaller NPs with thinner oxide shell is the criteria laid out by Zhang et al. [2] for being Kirkendall effect to be the reason for the formation of HNPs. At low fluence, the target exposed to outer wing of the laser beam will not participate in the NP formation as the energy would be comparable to

melting threshold energy. Therefore, thermal ablation will only be possible in the region that is exposed to the peak energy and hence would limit the yield. The presence of a smaller number of NPs in the medium would limit the inter-particle interaction, and the absence of this would limit the agglomeration, and hence, the size of NPs will be small. In addition, the fluence below the breakdown of the water will limit its reactivity, and hence, surface oxidation would be limited. As a result, shell thickness would be limited to 5–8 nm as shown in Fig. 2b. The presence of smaller NPs with thinner oxide shell suffices the criteria laid out by Zhang et al. [2] for the formation of HNPs via a Kirkendall effect. By performing the ablation in DI, its high thermal conductivity (0.591 WmK^{-1}) comes in handy whereby the NPs having intermediate morphology in the process of formation of HNPs can be seen. By carefully observing the morphology of synthesized NPs in the sample, we can trace the pathway of the formation of HNPs as shown in Fig. 3 along with schematics. As elaborated in Fig. 3, in the first step small-sized NPs will undergo surface oxidation, resulting into the core-shell morphology. Further, because of high reactivity of the Cu and longer ablation time of 60 min the partially oxidized surfaces of Cu NPs get sufficient time to interact with the dissolved O_2 molecules of DI. This initiates the diffusive oxidative reaction at the interface of Cu/Cu oxide [4, 18]. Since the diffusion rate of Cu metal is higher than Cu oxide (i.e., $J_{Cu} > J_{CuO}$), Cu core ions diffuse outward rapidly and the oxide shell diffuses inward slowly, creating void/vacancies at the metal side near Cu/Cu oxide interface [4, 18, 21]. The expansion of vacancy begins to form in the course of oxidative reaction and becomes larger as the metal core transfers to the oxide layer. Finally, the Cu core ions are completely consumed at the oxide layer, resulting in HNPs formation. Figure 2d shows the HRTEM image of single HNPs where the calculated d-spacing value of 0.23 nm indicates the (111) plane of monoclinic CuO phase. This

Fig. 3 Schematic growth mechanism of HNPs' generation at low laser fluence



observation reveals the formation of CuO HNPs, which are in confirmation with the above statement.

Further to establish the above given argument for the presence of HNPs, we performed the experiment at high fluence of 80 J/cm^2 . The TEM micrograph is shown in Fig. 4a. At higher fluence, agglomerated bigger-sized NPs with different morphologies (such as spherical, cubic and hexagonal shapes) are observed. The size of these particles is in the range of 25–70 nm. The morphological distribution of Cu particles as we have shown for low-fluence ablation in DI is not possible in the present situation because of agglomerated particles. The presence of bigger-sized NPs in DI had been discussed elaborately in our previous work [28]. For completeness, it has been attributed to the high fluence and the properties of DI. Contrary to low fluence, at high fluence we have observed NPs with multiple pores as shown in Fig. 4b.

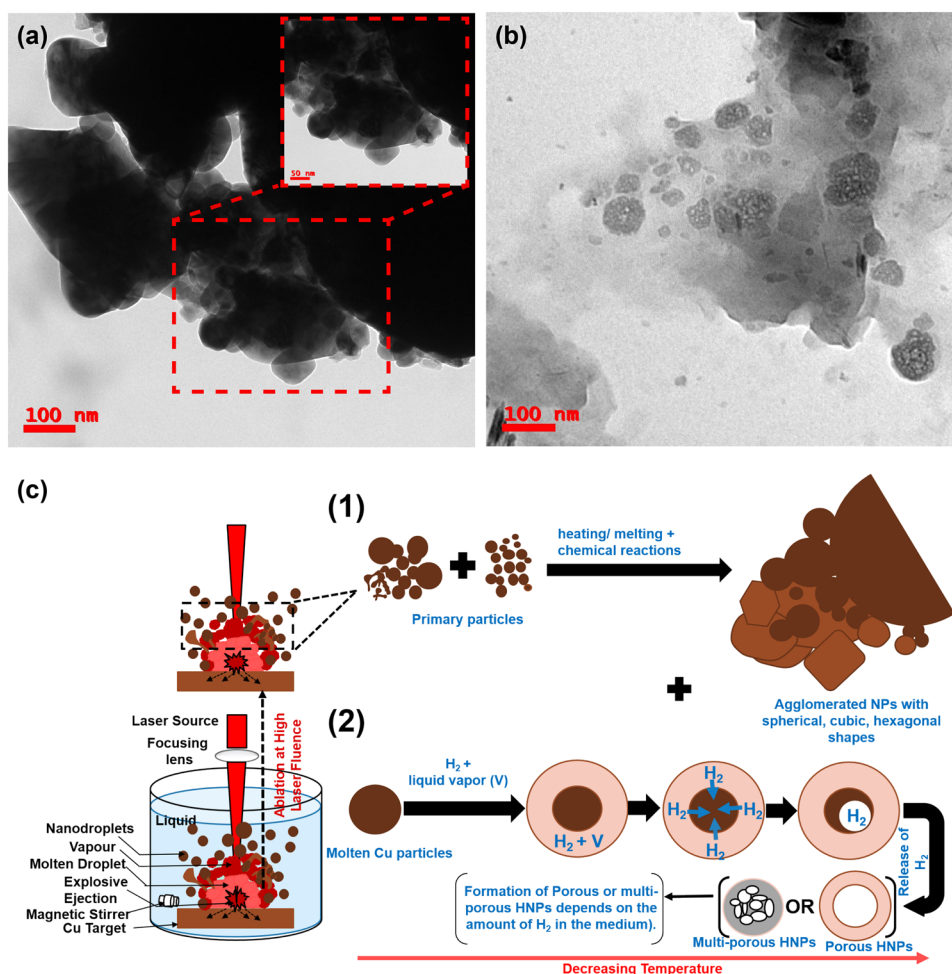
The presence of porous NPs at high fluence is because of dissolution of H_2 and consequently release of H_2 on saturation. As compared to low fluence, in this case the energy is above the threshold of optical breakdown of water [24], and hence, we will have ample amount of H_2 during ablation. The H_2 gas formed during thermal decomposition of DI

interacted with some molten Cu particles in the process of ablation. This interaction results in the formation of molten Cu core with an appearance of gas shell filled with H_2 and vapor of liquid. Recently, Kuzmin et al. [22] and Rawat et al. [28] reported the formation of HNPs of Al and Cu in ethanol where it is attributed to the enthalpy of H_2 dissolution in Al and Cu being endothermic in nature and hence make them efficient absorber of H_2 .

The size and number of holes in NPs are dependent on the amount of hydrogen in the medium according to the relation $P = DS$ [22], where ' P ' is the permeability, ' D ' is the diffusion coefficient and ' S ' is the solubility of hydrogen. The detailed schematics of the process is depicted in Fig. 4c-(2).

From the above experimental data and analysis, we concluded the following: (1) At low fluence, the formation of HNPs is because of the Kirkendall effect and the following pathway has been followed core \rightarrow core-shell and then via Kirkendall effect HNPs are formed. (2) At high fluence, energy above the breakdown threshold of DI, porous NPs were observed and has been attributed to the dissolution of H_2 and consequent release. Both of these experiments were carried out in DI, which is polar solvent and allows NPs to

Fig. 4 (a) and (b) TEM micrograph of Cu NPs synthesized at 60-min ablation with laser fluence of 80 J/cm^2 in DI. (c) Schematic growth mechanism of Cu NPs at high laser fluence



be readily oxidized. In addition, being hydrogen-saturated molecule at high fluence (above its optical breakdown) will make H_2 molecule readily available. To establish the proposed mechanism, the experiments were repeated in EG. As EG being oxygen-deficient solvent, the process of surface oxidation would be limited. It also acts as a capping solvent by forming electrical double layer (EDL) [29] on the surface. Having breakdown threshold more than the DI, the availability of H_2 molecules would be limited at high fluence. On ablating the Cu target at low fluence, the obtained micrographs are shown in Fig. 5a, b. Contrary to DI, no trace of HNPs was obtained on ablating the target with the fluence of $27 J/cm^2$. As mentioned above in the absence of oxidation process, manifestation of Kirkendall effect would be limited, hence restricting the formation of HNPs. We have mainly observed the large particulates with some trace of spherical NPs. This is because, at low fluence, the expulsion of melt from the surface will be limited due to its less lifetime of the bubble; the required pressure would not be able to build up. As a result, the melt will get re-solidified on the surface [11], which will be whirled out from the surface in the form of large particulates. Some of the particles because of high viscosity of EG (viscosity = 16.1 mPa s) remain in the focal region and encounter another pulse and get fragmented

to form small NPs as indicated with red dashed line arrow in Fig. 5b. At high fluence, the obtained micrographs are shown in Fig. 5c, d. Contrary to DI, no traces of HNPs or porous NPs were observed. Establishing the fact that for having porous NPs, it is important to have free hydrogen in the solvent. In this case, we have mainly observed NPs having spherical morphology with an average size of $3.4 \pm 0.1 \text{ nm}$ (inset of Fig. 5d). Contrary to DI, the particle size is smaller, which can be attributed to the physical properties of EG (i.e., high viscosity, high density ($\rho = 1.11 \text{ g/mL}$)) at high fluence [28].

3.1.2 XRD and SAED pattern Analysis

Figure 6a, b shows XRD patterns of immediately prepared samples synthesized at laser fluence of $27 J/cm^2$ and $80 J/cm^2$ in DI and EG for 60 min. At low-fluence ablation in DI and EG, we have observed single low-intensity Bragg's diffraction peak from Cu NPs at 2θ value of 43.4° , which correspond to (111) plane of fcc cubic structure. The presence of single peak is due to the low yield in the medium. To substantiate the obtained result at low fluence in both the media, we have performed SAED on the samples. As SAED being sensitive tool, a small number of NPs would be

Fig. 5 TEM micrographs of 60-min ablated Cu particles in EG synthesized with laser fluence of (a, b) $27 J/cm^2$ (c, d) $80 J/cm^2$. Inset in (d) shows the corresponding size distribution of Cu NPs

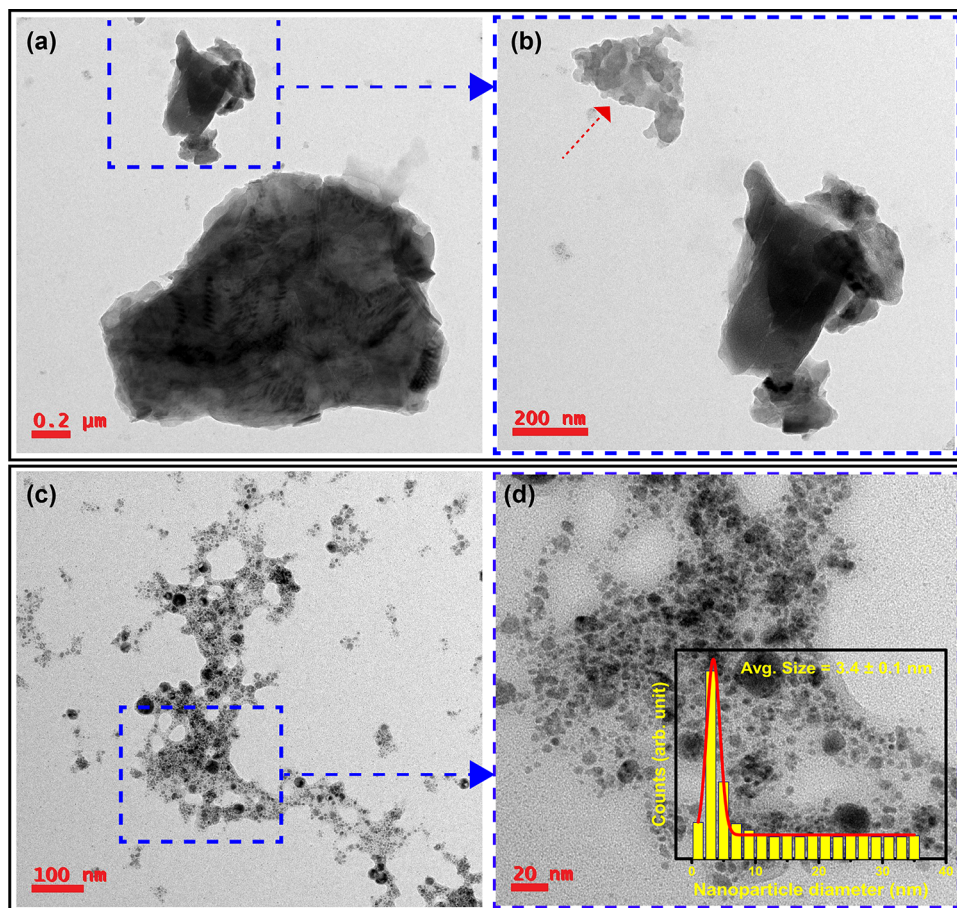
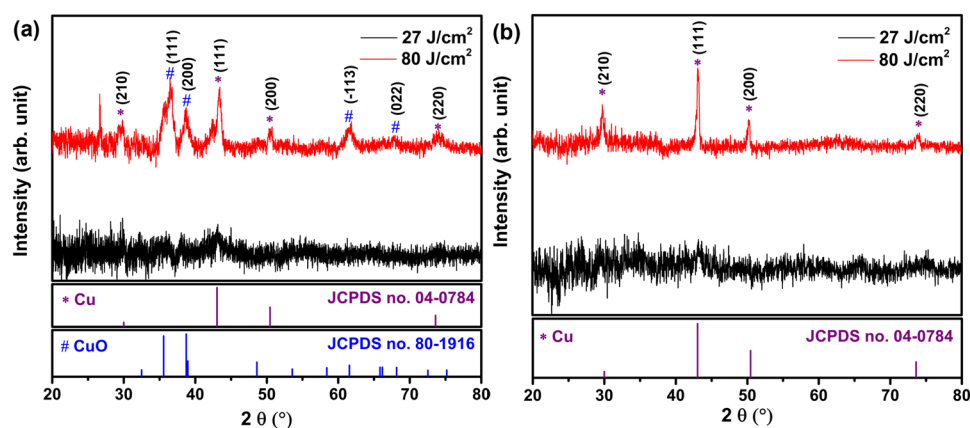


Fig. 6 XRD patterns of Cu/CuO NPs synthesized at laser fluence of 27 J/cm^2 and 80 J/cm^2 in (a) DI and (b) EG



enough to establish crystallinity and the phase transformation of the sample. The SAED patterns of colloidal solution of NPs in DI and EG are shown in Fig. 7a, b.

The SAED pattern analysis reveals the presence of (111), (210) crystalline planes of fcc cubic Cu NPs and (1-31) (-220), (220), (111) planes of monoclinic structure of CuO phase of NPs in DI. The corresponding interplanar d-spacing value of fcc and monoclinic phase of Cu and CuO NPs is obtained to be 0.20 nm, 0.30 nm and 0.10 nm, 0.13 nm, 0.14 nm, 0.23 nm, respectively [13, 28, 30]. Similarly, in EG the interplanar distances of 0.20 nm, 0.11 nm and 0.13 nm, 0.08 nm, 0.07 nm corresponding to lattice planes of (111), (-313) of fcc Cu NPs and (-220), (-331), (512) of monoclinic CuO NPs, respectively, were observed [13, 31]. The simultaneous presence of Cu/CuO phase indicates that the synthesized NPs are polycrystalline in nature.

At high fluence, more pronounced XRD peaks of Cu NPs at 29.8° , 43.4° , 50.5° and 73.9° were observed in DI, which correspond to (210), (111), (200) and (220) planes of cubic copper (JCPDS no.- 71-4610; 04-0784), respectively [13, 32, 33]. In addition, major diffraction peaks from CuO NPs phase were also observed. These peaks are at 35.6° , 38.7° ,

61.5° and 66.31° corresponding to (111), (200), (-113) and (022) (JCPDS no. 80-1916; 01-089-5896; 01-072-0629), respectively [10, 34–36]. However, in EG only the pure fcc phase of Cu NPs at 29.8° , 43.4° , 50.3° and 73.9° was observed. Contrary to DI, the monoclinic phase of CuO NPs was not seen in XRD. However, in SAED we have observed the presence of CuO. This can be attributed to the dependence on the sensitivity and accuracy of the instrument.

3.2 Optical analysis

3.2.1 UV–visible analysis

The absorption spectra of the sample ablated for 60 min with laser fluence of 27 J/cm^2 and 80 J/cm^2 in DI and EG are shown in Fig. 8a–d. Absorption spectrum of colloidal solution of Cu NPs synthesized at 27 J/cm^2 in DI was fitted with four peaks using the Gaussian fit method. The position of the peaks is P1(271 nm), P2(315 nm), P3(402 nm), and the surface plasmon resonance (SPR) peak is P4(618 nm) as shown in inset of Fig. 8a. With the increase in laser fluence, we observed a change in the intensity as well as differences

Fig. 7 SAED patterns of Cu/CuO NPs synthesized at laser fluence of 27 J/cm^2 in (a) DI and (b) EG

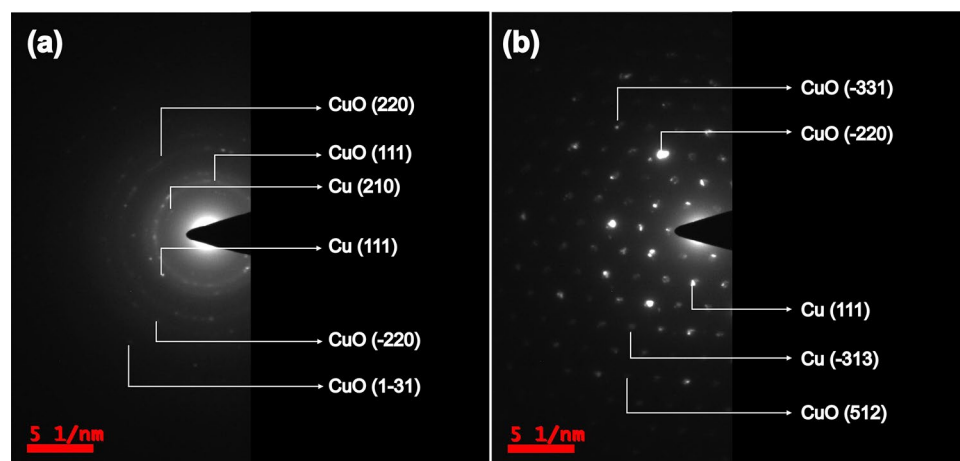
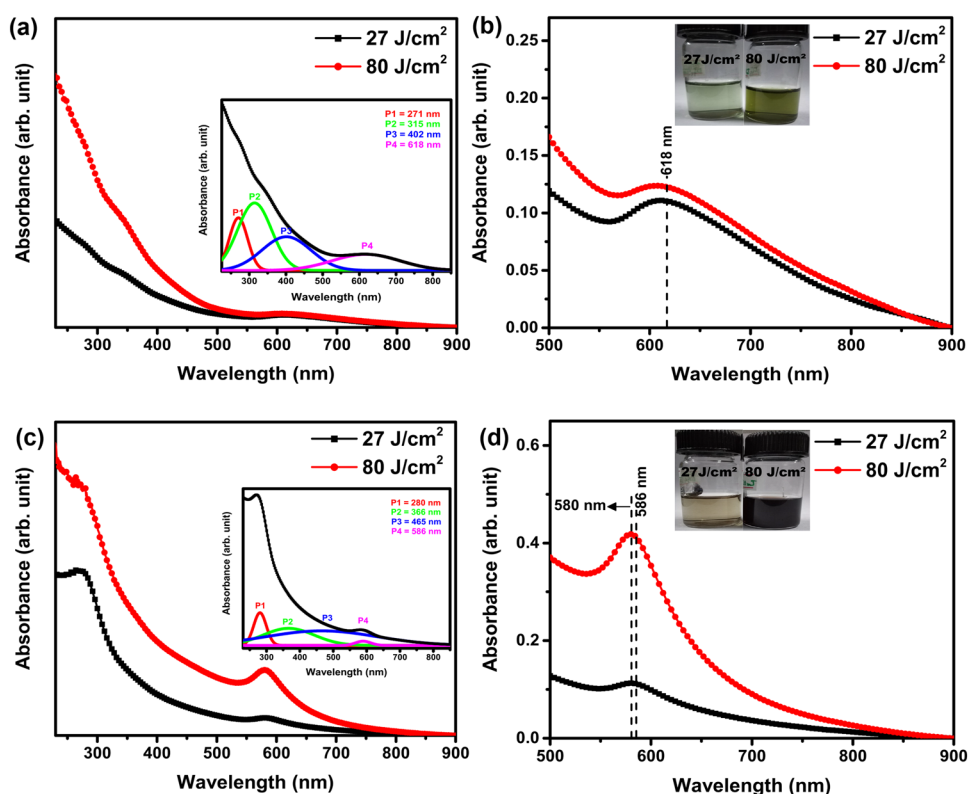


Fig. 8 UV–Vis spectra of Cu/CuO NPs synthesized at laser fluence of 27 J/cm^2 and 80 J/cm^2 in (a) DI. (b) Its corresponding SPR peaks and color change of the sample. (c and d) Absorption spectra of the sample synthesized in EG and their corresponding SPR peak and color indication

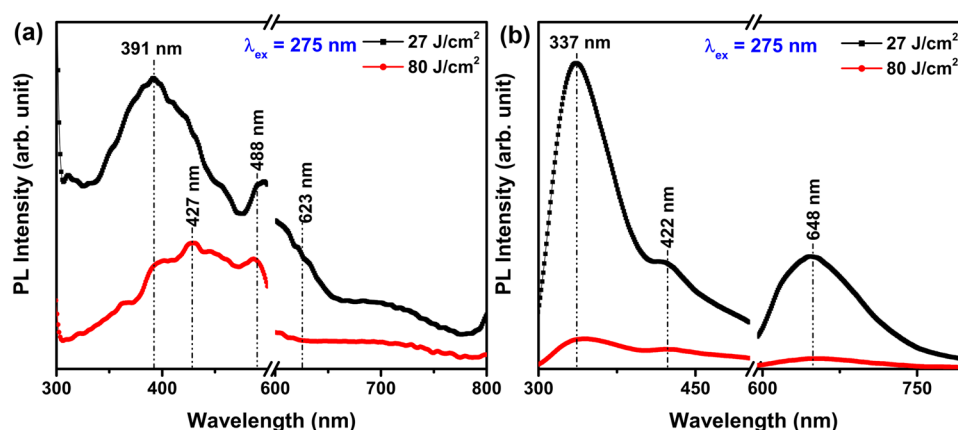


in the UV region on the absorption spectrum of the sample. The position of peak at P1 and P4 remains unchanged, but peaks P2 and P3 merge and a broad peak has appeared at 331 nm (data not shown). The peak P1 is attributed to the interband transition from the deep level of Cu atoms and its oxide [28, 37]. The broad peaks at P2 and P3 are assigned to the band edge absorption from CuO NPs and arise due to charge transition from oxygen to Cu ions [15, 28, 37, 38]. Broadness of P2 and P3 peaks at low fluence and their merging at high fluence can be attributed to the reduction in the size of CuO NPs or the presence of wide size distribution of the particles [10, 15, 39, 40]. SPR peak, P4 is broad and asymmetric in nature (as shown in Fig. 8b). The broadness and asymmetry of peak are attributed to the core-shell morphology present in DI [41]. With the increase in the fluence, no change in the position and the nature of peak are observed. This shows the presence of Cu@CuO NPs at high fluence, but due to high degree of agglomeration it is not observed in TEM micrographs. In the UV region, the considerable change in the spectra at high fluence is observed as compared to low fluence, which is attributed to the high concentration of CuO NPs in the sample. At high fluence, the laser-induced breakdown of the solvent at highly focused laser beam (as in our case) predominantly leads to the generation of CuO NPs [37]. Also, the change in the concentration of colloidal solution of NPs is clearly seen in the inset

of Fig. 8b, where light bluish color of the colloidal solution changes to dark greenish color.

Figure 8c shows the absorption spectra of Cu NPs ablated for 60 min in EG with 27 J/cm^2 and 80 J/cm^2 laser fluence. Similar to DI, here also we observed four peaks at P1 (280 nm), P2 (366 nm), P3 (465 nm) and P4 (586 nm). In comparison with DI, the peaks P1, P2 and P3 are broad and red-shifted, whereas SPR peak, P4, is blue-shifted. The broadness of the peaks retains same explanation as we did for DI case, and the blue shift of SPR peak is attributed to the presence of small-sized Cu NPs. On increasing the laser fluence, no appreciable change in the UV region was observed as was seen in DI case. The peak position of P1 remains unchanged, but the peaks P2, P3 and P4 are shifted toward low wavelength region, i.e., at 324 nm, 450 nm and 580 nm. Contrary to DI, in EG we observed the narrowing and the enhancement of SPR peak, which is attributed to the high concentration of Cu NPs. As EG being oxygen-deficient molecules, the synthesis of CuO or Cu@CuO NPs will be limited. In addition, as EG being viscous, most of the large-sized particulates will undergo fragmentation giving rise to uniformly sized Cu NPs, resulting in the narrowing of SPR peak. Inset of Fig. 8d clearly indicates the change of color of colloidal solution of Cu NPs from light brownish to wine red color.

Fig. 9 PL spectra of Cu/CuO NPs dispersed in (a) DI and (b) EG



3.2.2 PL analysis

Figure 9a, b shows the PL spectra of colloidal solution of Cu/CuO NPs synthesized at 27 J/cm² and 80 J/cm² for 60 min in DI and EG, respectively. To eliminate the signal appearing in the emission corresponding to the second harmonic of the excitation, both the graphs have been plotted with break. In Fig. 9a, the emission spectra of sample in DI recorded at the excitation wavelength of 275 nm are shown. On exciting the sample with 275 nm, we have observed emission peaks at 391 nm, 488 nm and 623 nm. The sharp and intense peak at 391 nm (3.2 eV) is attributed to the direct band edge emission arising from CuO NPs because of the electrons and holes recombination in CuO [38, 42], which are in confirmation with the calculated band gap value of 3.85 eV as shown in supplementary Figure S2(a). The peak at 488 nm (2.54 eV) is attributed to defect states originating from the emission mediated between oxygen vacancies and Cu interstitials [38]. The shoulder emission peak at 623 nm (1.99 eV) is attributed to the interband transition between sp-conduction band and d band of Cu NPs. Further, Das et al. and Rawat et al. reported that the origin of this peak is due to the intra-band transition within sp conduction (i.e., HOMO–LOMO transition) triggered under the excitation wavelength range between 240 and 270 nm [28, 33]. For confirmation, we have excited the samples with 360 nm and 420 nm (absorption peaks of CuO NPs) and have observed the suppression of emission peak at 623 nm. The emission spectra are shown in supplementary figure S3. For higher laser fluence, the band edge emission of CuO NPs shifted toward the red region and appeared at 427 nm (2.90 eV). The emission peak at 427 nm is less intense and broad and the peak at 623 nm get disappeared. Peak at 427 nm is attributed to the indirect interband transition arising from the presence of valence defects in the synthesized NPs [43–45].

Subsequently, the PL spectrum of the samples synthesized in EG with 27 J/cm² and 80 J/cm² of laser fluence for 60 min is shown in Fig. 9b. Under the excitation of samples

with 275 nm, a sharp and intense peak at ~ 337 nm (3.67 eV) is observed together with shoulder and broad peaks at 422 nm (2.93 eV) and 648 nm (1.91 eV). The sharp band edge emission from CuO NPs is in agreement with the calculated band gap value of 3.70 eV [as shown in figure S2 (b)]. Contrary to DI, the band edge and defect emission peaks are blue-shifted, whereas the peak related to intraband transition is red-shifted. The blue shift and red shift in the emission spectrum are because of the decrease and increase in the size of NPs, respectively. On increasing the laser fluence to 80 J/cm², the emission peak intensity of these peaks gets suppressed and the peaks get broader. The suppression and broadness of the emission peaks can be attributed to the presence of small-sized NPs with large number of defects [42, 46]. It is noted that the liquid environment plays a crucial role in optimizing the size and defects state of Cu and its oxide NPs, which need further investigation.

4 Conclusion

Nanosecond pulsed laser operating at 1064 nm (8-ns pulse duration) and fluence of 27 J/cm² (low) and 80 J/cm² (high) was used to ablate Cu target immersed in two different solvents, viz. DI and EG. At low and high laser fluence, ablation of Cu target in DI results in the formation of HNPs and porous NPs, respectively. At low fluence, HNPs are formed via Kirkendall effect, whereas at high fluence, it is the result of dissolution of H₂ and their consequent release on saturation. In EG, no signature of hollow or porous NPs was seen at both fluences. This is because EG being oxygen-deficient and viscous in nature limits the formation of CuO and Cu@CuO NPs at low fluence. At high fluence, because of being viscous the process of photofragmentation prevails giving rise to small-sized Cu NPs.

Acknowledgements R. Rawat greatly acknowledges the grant from RGNF-UGC, Government of India. A. Tiwari and A. Tripathi would like to thankfully acknowledge the financial assistance from IUAC, New Delhi. N. Arun thanks UGC for NET research fellowship. We thank Central Facility for Nanotechnology (CFN), University of Hyderabad, for the usage of TEM facilities.

References

1. D. Zhang, B. Gokce, S. Barcikowski, *Chem. Rev.* **117**(5), 3990 (2017)
2. T. Zhang, Z. Wang, D.J. Hwang, *Appl. Phys. A* **123**(10), 616 (2017)
3. T. Gao, B.P. Jelle, L.I.C. Sandberg, A. Gustavsen, A.C.S. Appl. Mater. Interfaces **5**(3), 761 (2013)
4. H.J. Fan, U. Gösele, M. Zacharias, *Small* **3**(10), 1660 (2007)
5. S. Sun, Q. Yang, S. Liang, Z. Yang, *Cryst. Eng. Comm.* **19**(42), 6225 (2017)
6. Z. Yan, D.B. Chrisey, *J. Photochem. Photobiol. C* **13**(3), 204 (2012)
7. X. Liu, J. Chen, P. Liu, H. Zhang, G. Li, T. An, H. Zhao, *Appl. Catal. A* **521**, 34 (2016)
8. V. Amendola, M. Meneghetti, *Phys. Chem. Chem. Phys.* **15**(9), 3027 (2013)
9. P.K. Baruah, A.K. Sharma, A. Khare, *RSC Adv.* **9**(26), 15124 (2019)
10. B.E.B. Al-Jumaili, Z.A. Talib, A. Zakaria, A. Ramizy, N.M. Ahmed, S.B. Paiman, J.L. Ying, I.B. Muhd, H. Baqiah, *Appl. Phys. A* **124**(9), 577 (2018)
11. R. Rawat, A. Tiwari, V. Vendamani, A. Pathak, S.V. Rao, A. Tripathi, *Opt. Mater.* **75**, 350 (2018)
12. K. Choudhury, R. Singh, P. Kumar, M. Ranjan, A. Srivastava, A. Kumar, *Nano-Struct. Nano-Objects* **17**, 129 (2019)
13. H. Desarkar, P. Kumbhakar, A. Mitra, *Appl. Nanosci.* **2**(3), 285 (2012)
14. M. Dell'Aglio, R. Gaudioso, O. De Pascale, A. De Giacomo, *Appl. Surf. Sci.* **348**, 4 (2015)
15. M. Gondal, T.F. Qahtan, M.A. Dastageer, T.A. Saleh, Y.W. Maganda, D.H. Anjum, *Appl. Surf. Sci.* **286**, 149 (2013)
16. C.G. Moura, R.S.F. Pereira, M. Andritschky, A.L.B. Lopes, J.P. de Freitas Grilo, R.M. do Nascimento, F.S. Silva, *Opt. Laser Technol.* **97**, 20 (2017)
17. E. Solati, L. Dejam, D. Dorrnanian, *Opt. Laser Technol.* **58**, 26 (2014)
18. R. Nakamura, D. Tokozakura, H. Nakajima, J.G. Lee, H. Mori, *J. Appl. Phys.* **101**(7), 074303 (2007)
19. C.M. Wang, D.R. Baer, L.E. Thomas, J.E. Amonette, J. Antony, Y. Qiang, G. Duscher, *J. Appl. Phys.* **98**(9), 094308 (2005)
20. Y. Yin, R.M. Rioux, C.K. Erdonmez, S. Hughes, G.A. Somorjai, A.P. Alivisatos, *Science* **304**(5671), 711 (2004)
21. K. Niu, J. Yang, S. Kulinich, J. Sun, X. Du, *Langmuir* **26**(22), 16652 (2010)
22. P. Kuzmin, G. Shafeev, G. Viau, B. Warot-Fonrose, M. Barberoglou, E. Stratakis, C. Fotakis, *Appl. Surf. Sci.* **258**(23), 9283 (2012)
23. Z. Yan, R. Bao, R.N. Wright, D.B. Chrisey, *Appl. Phys. Lett.* **97**(12), 124106 (2010)
24. Z. Yan, R. Bao, Y. Huang, D.B. Chrisey, *J. Phys. Chem. C* **114**(26), 11370 (2010)
25. Z. Yan, R. Bao, C.M. Busta, D.B. Chrisey, *Nanotechnology* **22**(26), 265610 (2011)
26. D.A. Goncharova, T.S. Kharlamova, I.N. Lapin, V.A. Svetlichnyi, *J. Phys. Chem. C* **123**(35), 21731–21742 (2019)
27. K. Zhang, R.A. Ganeev, G.S. Boltaev, C. Guo, *Appl. Phys. A* **125**(10), 698 (2019)
28. R. Rawat, A. Tiwari, N. Arun, S.N. Rao, A.P. Pathak, A. Tripathi, *Chem. Select* **4**(35), 10471 (2019)
29. J. Polte, *Cryst. Eng. Comm.* **17**(36), 6809 (2015)
30. A. Sahai, N. Goswami, M. Mishra, G. Gupta, *Ceram. Int.* **44**(2), 2478 (2018)
31. D. Paul Joseph, C. Venkateswaran, R. Selva Vennila, *Adv. Mater. Sci. Eng.* **2010**, 1–14 (2010)
32. K. Cheirnadurai, S. Biswas, R. Murali, P. Thanikaivelan, *RSC Adv.* **4**(37), 19507 (2014)
33. R. Das, S.S. Nath, R. Bhattacharjee, *J. Lumin.* **131**(12), 2703 (2011)
34. P. Yugandhar, T. Vasavi, P.U.M. Devi, N. Savithramma, *Appl. Nanosci.* **7**(7), 417 (2017)
35. P.V. Kumar, U. Shameem, P. Kollu, R. Kalyani, S. Pammi, *J. Bio-nanosci.* **5**(3), 135 (2015)
36. M. Verma, V. Kumar, A. Katoch, *Mater. Sci. Semicond. Process.* **76**, 55 (2018)
37. A. Nath, A. Khare, *J. Appl. Phys.* **110**(4), 043111 (2011)
38. A. El-Trass, H. ElShamy, I. El-Mehasseb, M. El-Kemary, *Appl. Surf. Sci.* **258**(7), 2997 (2012)
39. A. Sahai, N. Goswami, S. Kaushik, S. Tripathi, *Appl. Surf. Sci.* **390**, 974 (2016)
40. W. Chen, J. Chen, Y.B. Feng, L. Hong, Q.Y. Chen, L.F. Wu, X.H. Lin, X.H. Xia, *Analyst* **137**(7), 1706 (2012)
41. P.K. Baruah, A.K. Sharma, A. Khare, *Opt. Laser Technol.* **108**, 574 (2018)
42. S. Dagher, Y. Haik, A.I. Ayesh, N. Tit, *J. Lumin.* **151**, 149 (2014)
43. H. Siddiqui, M. Qureshi, F.Z. Haque, *Optik Int. J. Light Electron Opt.* **127**(5), 2740 (2016)
44. C. Tamuly, I. Saikia, M. Hazarika, M.R. Das, *RSC Adv.* **4**(95), 53229 (2014)
45. P. Chand, A. Gaur, A. Kumar, U.K. Gaur, *Mater. Sci. Semicond. Process.* **38**, 72 (2015)
46. S. Rehman, A. Mumtaz, S. Hasanain, *J. Nanopart. Res.* **13**(6), 2497 (2011)

Publisher's Note Springer Nature remains neutral with regard to jurisdictional claims in published maps and institutional affiliations.

Terms and Conditions

Springer Nature journal content, brought to you courtesy of Springer Nature Customer Service Center GmbH (“Springer Nature”).

Springer Nature supports a reasonable amount of sharing of research papers by authors, subscribers and authorised users (“Users”), for small-scale personal, non-commercial use provided that all copyright, trade and service marks and other proprietary notices are maintained. By accessing, sharing, receiving or otherwise using the Springer Nature journal content you agree to these terms of use (“Terms”). For these purposes, Springer Nature considers academic use (by researchers and students) to be non-commercial.

These Terms are supplementary and will apply in addition to any applicable website terms and conditions, a relevant site licence or a personal subscription. These Terms will prevail over any conflict or ambiguity with regards to the relevant terms, a site licence or a personal subscription (to the extent of the conflict or ambiguity only). For Creative Commons-licensed articles, the terms of the Creative Commons license used will apply.

We collect and use personal data to provide access to the Springer Nature journal content. We may also use these personal data internally within ResearchGate and Springer Nature and as agreed share it, in an anonymised way, for purposes of tracking, analysis and reporting. We will not otherwise disclose your personal data outside the ResearchGate or the Springer Nature group of companies unless we have your permission as detailed in the Privacy Policy.

While Users may use the Springer Nature journal content for small scale, personal non-commercial use, it is important to note that Users may not:

1. use such content for the purpose of providing other users with access on a regular or large scale basis or as a means to circumvent access control;
2. use such content where to do so would be considered a criminal or statutory offence in any jurisdiction, or gives rise to civil liability, or is otherwise unlawful;
3. falsely or misleadingly imply or suggest endorsement, approval, sponsorship, or association unless explicitly agreed to by Springer Nature in writing;
4. use bots or other automated methods to access the content or redirect messages
5. override any security feature or exclusionary protocol; or
6. share the content in order to create substitute for Springer Nature products or services or a systematic database of Springer Nature journal content.

In line with the restriction against commercial use, Springer Nature does not permit the creation of a product or service that creates revenue, royalties, rent or income from our content or its inclusion as part of a paid for service or for other commercial gain. Springer Nature journal content cannot be used for inter-library loans and librarians may not upload Springer Nature journal content on a large scale into their, or any other, institutional repository.

These terms of use are reviewed regularly and may be amended at any time. Springer Nature is not obligated to publish any information or content on this website and may remove it or features or functionality at our sole discretion, at any time with or without notice. Springer Nature may revoke this licence to you at any time and remove access to any copies of the Springer Nature journal content which have been saved.

To the fullest extent permitted by law, Springer Nature makes no warranties, representations or guarantees to Users, either express or implied with respect to the Springer nature journal content and all parties disclaim and waive any implied warranties or warranties imposed by law, including merchantability or fitness for any particular purpose.

Please note that these rights do not automatically extend to content, data or other material published by Springer Nature that may be licensed from third parties.

If you would like to use or distribute our Springer Nature journal content to a wider audience or on a regular basis or in any other manner not expressly permitted by these Terms, please contact Springer Nature at

onlineservice@springernature.com